Failure Probability Constrained AC Optimal Power Flow

Anirudh Subramanyam, Jacob Roth, and Mihai Anitescu, *Member, IEEE*

***Abstract*—Despite cascading failures being the central cause of blackouts in power transmission systems, existing operational and planning decisions are made largely by ignoring their underlying cascade potential. This paper posits a reliability-aware AC Optimal Power Flow formulation that seeks to design a dispatch point which has a low operator-specified likelihood of triggering a cascade starting from any single component outage. By exploiting a recently developed analytical model of the probability of component failure, our Failure Probability-constrained ACOPF (FP-ACOPF) utilizes the system's expected first failure time as a smoothly tunable and interpretable signature of cascade risk. We use techniques from bilevel optimization and numerical linear algebra to efficiently formulate and solve the FP-ACOPF using off-the-shelf solvers. Simulations on the IEEE 118-bus case show that, when compared to the unconstrained and N-1 security-constrained ACOPF, our probability-constrained dispatch points can delay the expected onset of cascades and reduce the probability of long severe cascades, by more than ten and two orders of magnitude, respectively, while incurring less than 1% higher generation costs and load shedding.**

***Index Terms*—cascading failures, AC optimal power flow**

I. Introduction

A cascading failure in a power transmission system refers to a sequence of dependent outages of individual system components that successively disable parts of the grid, leading to a significant loss of served power or large blackout in the worst case. Accounts of major blackouts reveal that cascading failures are often triggered by an initial event that is largely unpredictable (such as extreme weather) but are sustained by subsequent events that are causally linked via Kirchhoff's laws and automatic control actions of protection devices. For example, the outage of a single component can lead to redistribution of power flows in the remainder of the network in a way that can cause large overcurrents on some transmission lines. This, in turn, may trigger protection relays to disconnect these lines automatically if the current flow exceeds some threshold rating, or it may lead to eventual thermal failure if the overcurrents remain sustained for a long time.

The large direct and indirect costs associated with blackouts, along with mandatory standards set forth by the North American Electric Reliability Corporation (NERC) to address cascading outages, have motivated the development of a plethora of tools for the simulation and analysis of cascading failures; see reviews [1], [2] and references therein. These tools can be broadly classified as *(a)* complex networks approaches that consider the pure topological properties of power networks while ignoring or simplifying the underlying physics (e.g., see [3], [4]), *(b)* quasi-steady-state (e.g., see [5], [6]) or dynamic (e.g., see [7]–[9]) methodologies which combine physics-based DC or AC power flow models with Monte Carlo or enumerative sampling methods, and *(c)* high-level statistical models built either on historical/simulation data or on simplified power system physics (e.g., see [10], [11]).

The authors are with the Mathematics and Computer Science Division, Argonne National Laboratory, Lemont IL 60439.

While these tools have proved immensely useful in deepening our understanding of cascading failures, their use for risk mitigation and decision-making have been largely restricted to limiting the propagation of a cascading failure, e.g., via controlled load shedding or intentional islanding, *after* severe contingencies have already occurred (e.g., see [12]–[14]). Existing practices for the prevention of cascading failures *before* they occur, by tuning and modifying the controllable properties of the power network, has largely relied upon $N-k$ security criteria and simulation-based contingency analyses as notional surrogates for reducing cascading likelihood.

Although simulation-based tools can influence long-term cascade mitigation solutions, such as line capacity or generator margin allocations and protection system enhancements (e.g., see [15]–[17]), they are fundamentally limited in preventing cascades in short-term operations such as economic dispatch or optimal power flow. This is because they do not provide any direct functional relationship between control parameters and cascade potential, or they entail expensive Monte Carlo sampling and numerical integration requirments and are thus challenging to incorporate within optimization algorithms.

This work proposes to incorporate in the classical ACOPF model, an analytical – as opposed to simulation-based – model of cascade severity that is an *explicit function* of the network properties and dispatch point. In contrast to existing methods, we aim to determine a dispatch point subject to the constraint that the *probability of individual component failure* remains below an operator-prescribed threshold. Our model capitalizes upon results from [18], which in contrast to other approaches for simulating cascading failures, provides an *analytic expression* for the failure probability as a function of the dispatch point. This is achieved by modeling *Gaussian load and generation fluctuations* in the AC power flow dynamics, and interpreting the latter as the diffusion of a particle in an energy landscape subject to stochastic forcing. Large deviations theory then provides the means to analytically relate the failure probability to the underlying energy surface.

For a given system state (consisting of voltages and power flows) at equilibrium, the analytical expression for the failure probability of an individual component requires solving a nonlinear optimization problem that computes a "most likely" failure state starting from this equilibrium state. However, since

the latter is contingent on the dispatch point, explicitly constraining the failure probability of an *individual component*, or of a *cascading sequence of multiple components*, is tantamount to solving a bilevel optimization problem. We settle for the former and demonstrate that constraining individual failure probabilities, which is equivalent to increasing the system's expected first failure time–or decreasing its *failure rate*–is a safe approximation and effective surrogate for constraining the probability of a cascading failure sequence. Solving the bilevel model, however, is computationally challenging since it is nonlinear, nonconvex, and involves eigenvalues and determinants of high-dimensional matrices that scale with the network size. Nevertheless, we show that this eigenvalue- and determinant-constrained model can be reformulated entirely algebraically and solved efficiently using standard solvers, if we exploit the low-rank nature of the failure constraints along with the first- and second-order optimality conditions of the nested problem.

Our key finding is that it is possible to modify the dispatch point so as to satisfy a prescribed threshold of failure probability. Specifically, the system's expected first failure time, and hence, the probability of cascading over a given time horizon, can be improved by *several orders of magnitude*, without incurring vastly higher generation costs or load shedding.

We believe this is the first work that allows such principled control of cascading risk in operational dispatch. Although it can be viewed as a probabilistic $N-1$ variant, our approach offers several advantages over classical $N-k$ models. The first crucial difference is that, by tuning the system's *failure rate limit*, we can systematically and *smoothly* explore the trade-offs between cascade potential, dispatch costs and operator conservatism, at *no significant increase in computational complexity*. In contrast, $N-k$ approaches must resort to a non-smooth control of k to achieve the same objective, while invariably incurring a sharp increase in combinatorial complexity. Another subtle, yet practically useful, advantage of our approach is its *interpretability*. Indeed, the benefit (in terms of reliability) of increasing k in $N-k$ approaches, is difficult to convey outside the domain. Our approach, on the other hand, allows the system operator to decide between a *failure rate limit* of $10^{-6}s^{-1}$ or $10^{-15}s^{-1}$ (for example), which is equivalent to deciding between observing the first failure once every 10^6 or 10^{15} seconds. This is a statement that is better aligned with the philosophy of regulatory constraints which tend to be in occurrences per unit of time.

This paper is organized as follows. Section II presents assumptions, and reviews the probabilistic failure model of [18]. Section III presents the failure probability-constrained ACOPF model along with its reformulation. Section IV demonstrates the empirical performance of our method and Section V offers concluding remarks and directions for future work.

II. Failure Probability Model

A. Notation

We use $\mathcal{N} = \{1,\dots,n_b\}$ to denote the set of buses, and $\mathcal{L} \subseteq \mathcal{N}\times\mathcal{N}$ to denote the set of transmission lines, where $l=(i,j)\in\mathcal{L}$ is a line from bus i and to bus j. We denote the set of generators by $\mathcal{G} = \{1,\dots,n_g\}$, and let $\mathcal{G}_i$ be the set of generators connected to bus $i\in\mathcal{N}$; note that $\mathcal{G}=\cup_{i\in\mathcal{N}}\mathcal{G}_i$. For ease of notation, we define $\mathcal{N}' \coloneqq \{i\in\mathcal{N} : \mathcal{G}_i=\emptyset\}$ to denote the set of non-generator buses, *i.e.*, those that are not connected to any generator and similarly, $\mathcal{L}' \coloneqq \{(i,j)\in\mathcal{L} : \mathcal{G}_i=\emptyset \text{ or } \mathcal{G}_j=\emptyset\}$ to denote the set of lines that are connected to at least one non-generator bus. The nodal admittance matrix $Y=G+\sqrt{-1}B\in\mathbb{C}^{n_b\times n_b}$ with conductance and susceptance matrices $G\in\mathbb{R}^{n_b\times n_b}$ and $B\in\mathbb{R}^{n_b\times n_b}$, respectively.

We denote active and reactive power generations by $p_g, q_g \in \mathbb{R}^{n_g}$, active and reactive power demands by $p_d, q_d\in\mathbb{R}^{n_b}$, and net active and reactive powers by $p_{net}, q_{net}\in\mathbb{R}^{n_b}$, where we define $p_{net,i} \coloneqq p_{d,i} - \sum_{k\in\mathcal{G}_i} p_{g,k}$ and $q_{net,i} \coloneqq q_{d,i} - \sum_{k\in\mathcal{G}_i} q_{g,k}$ for $i\in\mathcal{N}$. The voltage magnitudes and angles are denoted by $V\in\mathbb{R}^{n_b}$ and $\theta\in\mathbb{R}^{n_b}$.

For a vector $z\in\mathbb{C}^n$, we use $\|z\|$ and z^* to denote its Euclidean norm and Hermitian transpose, respectively, and we use e^z and $\log(z)$ to denote the vectors $(e^{z_1},\dots,e^{z_n})\in\mathbb{C}^n$ and $(\log(z_1),\dots,\log(z_n))\in\mathbb{C}^n$. Given vectors $z,\tilde{z}\in\mathbb{C}^n$, we use $z\circ\tilde{z}$ to denote the Hadamard product $(z_1\tilde{z}_i,\dots,z_n\tilde{z}_n)\in\mathbb{C}^n$. For a matrix $A\in\mathbb{C}^{n\times n}$, we use $\rho(A)$, $\det(A)$, and $\mathrm{adj}(A)$ to denote its spectral radius, determinant and adjugate, respectively, and $A\succ 0$ ($\succeq 0$) to indicate that it is positive definite (semi-definite). For a given matrix $A\succeq 0$ and vector $z\in\mathbb{C}^n$, we use $\|z\|_A$ to denote $\sqrt{z^*Az}$.

In formulating the probability model, it will be convenient to divide the power generations and voltages $(p_g,q_g,V,\theta)\in\mathbb{R}^m$ ($m\coloneqq 2n_g+2n_b$) into two distinct sets. After selecting an arbitrary generator bus $\sigma\in\mathcal{N}\setminus\mathcal{N}'$ as the slack bus in the steady-state context and reference bus in the dynamics context, we collect all voltage magnitudes at non-generator buses and voltage angles at non-slack buses in the state vector $x=\big(\{V_i\}_{i\in\mathcal{N}'},\{\theta_i\}_{i\in\mathcal{N}\setminus\{\sigma\}}\big)\in\mathbb{R}^d$, $d=|\mathcal{N}'|+|\mathcal{N}|-1$. The remaining voltage components and power generations are aggregated in the vector $y=\big(\{V_i\}_{i\in\mathcal{N}\setminus\mathcal{N}'},\theta_\sigma,p_g,q_g\big)\in\mathbb{R}^{m-d}$.

B. Assumptions

Motivated by the automatic control actions of protection relays, we assume that individual system components fail in a deterministic manner according to a component-specific state equation. Specifically, we assume that a component, such as a transmission line $l\in\mathcal{L}$, fails if the value of a certain function $\Theta_l:\mathbb{R}^m\mapsto\mathbb{R}$ at the current state (x,y) exceeds a critical value $\Theta_l^{\max}$. Furthermore, we assume that after failure, a component remains failed over the entire dispatch horizon of the ACOPF.

The algebraic state functions Θ can be used to model various component failures, such as under-voltage conditions at buses or line surges in transformers. For the remainder of the paper, however, we assume that component failures occur only due to current overloads in transmission lines $l=(i,j)\in\mathcal{L}$ beyond an emergency rating I_l^{trip}: (here, $\Theta_l^{\max}\coloneqq(I_l^{\mathrm{trip}})^2$)

$$\Theta_l(x,y) = |Y_{ij}|^2\left(V_i^2+V_j^2-2V_iV_j\cos(\theta_i-\theta_j)\right) \qquad (1)$$

This is partly because it simplifies the exposition, and partly because the corresponding failure model has already been studied and validated against real cascade data in [18], [19]. We note, however, that the methodology does not preclude us from considering other failure mechanisms.

In addition, we shall assume that *(i)* the network is lossless[1], *i.e.*, $G = 0$, *(ii)* transmission line failures are induced only by fluctuations in active and reactive power demand and active power generation (rather than exogenous events), and therefore, *(iii)* only the subset $\mathcal{L}'$ of transmission lines that connect to at least one non-generator bus have a nonzero likelihood of failing over the dispatch horizon of the ACOPF.

C. Analytical model of line failures

We model the grid's electro-mechanical behavior using a system of stochastic differential equations (SDE), by introducing a scalar noise parameter $\tau > 0$ into the following variant[2] of the standard, structure-preserving model [21]–[25]:

$$\mathrm{d}x_t^\tau = (J - S)\nabla_x \mathcal{H}(x_t^\tau, y)\mathrm{d}t + \sqrt{2\tau S}\mathrm{d}W_t. \tag{2}$$

Here, $x_t^\tau \in \mathbb{R}^d$ denotes the system state at time t, J and S represent appropriate system matrices [18], W_t is a d-dimensional vector of independent Wiener processes, and $\mathcal{H}$ is the following energy function [18], [19], [21] that is obtained as the first integral of the deterministic dynamics[3]:

$$\mathcal{H}(x, y) \coloneqq \tfrac{1}{2}(V \circ e^{\mathrm{i}\theta})^* \, Y \, (V \circ e^{\mathrm{i}\theta}) + p_{net}^\top \theta + q_{net}^\top \log(V) \tag{3}$$

It is worth pointing out that (3) is closely related to the widely-used transient stability analysis energy function [26]; similar to the latter, which is used to measure distance to instability, we use (3) to assess the probability of the stochastically perturbed dynamics reaching a triggering surface.

We note that the vector y is assumed to have been fixed to appropriate values *a priori*, and we shall return to choosing a value for y in the subsequent section when we describe the ACOPF formulation. For now, observe that the structure of the energy function (3) ensures that, for any specified value of y, any point $x \in \mathbb{R}^d$ that satisfies $\nabla_x \mathcal{H}(x, y) = 0$ is a solution to the lossless power flow equations:

$$p_{net,i} + \sum_{j \in \mathcal{N}} B_{ij} V_i V_j \sin(\theta_i - \theta_j) = 0, \quad i \in \mathcal{N}, \tag{4}$$

$$q_{net,i} - \sum_{j \in \mathcal{N}} B_{ij} V_i V_j \cos(\theta_i - \theta_j) = 0, \quad i \in \mathcal{N}. \tag{5}$$

In particular, any local energy minimizer,

$$\bar{x}(y) \in \operatorname*{arg\,min}_{x \in \mathbb{R}^d} \mathcal{H}(x, y) \tag{6}$$

defines a feasible solution to (4), (5) and serves as a stable equilibrium for the network dynamics defined by y. To simplify notation, we drop the dependence of $\bar{x}$ on y in the remainder of the paper.

Under the SDE model (2) initialized at $x_0^\tau = \bar{x}$, the failure probability of a line $l \in \mathcal{L}'$ (considered in isolation from the rest of the network) can be quantified by its so-called *first passage time*. The latter is defined to be the first time at which the system state x_t^τ triggers the failure condition (1) for line l. Assuming $\Theta_l(\bar{x}, y) < \Theta_l^{\max}$, this is equivalent to

$$T_l^\tau(y) \coloneqq \inf\{t > 0 : \Theta_l(x_t^\tau, y) \geq \Theta_l^{\max}\}. \tag{7}$$

By exploiting results from large deviations theory [27], [28], it was shown in [18] that, as $\tau \to 0$, $T_l^\tau(y)$ is an exponential random variable whose mean satisfies the following relation:

$$\lim_{\tau \to 0} \tau \log\left(\mathbb{E}\left[T_l^\tau(y)\right]\right) = \min_{x : \Theta_l(x_t^\tau, y) = \Theta_l^{\max}} \mathcal{H}(x, y) - \mathcal{H}(\bar{x}, y) \tag{8}$$

A point at which the minimum is obtained is called the *most likely failure point* and is defined as

$$x_l^\star(y) \coloneqq \operatorname*{arg\,min}_{x \in \mathbb{R}^d} \left\{\mathcal{H}(x, y) : \Theta_l(x, y) = \Theta_l^{\max}\right\}, \tag{9}$$

where we have implicitly assumed $x_l^\star$ to be unique[4]. As before, we drop the dependence of $x_l^\star$ on y to simplify notation.

For finite values of τ, we can thus use relation (8) to compute a log-approximate *failure rate* (*i.e.*, the reciprocal of the mean failure time). In addition to this log-approximation, a subexponential correction to the failure rate was also obtained in [18] yielding the following expressions:

$$\lambda_l^\tau(y) \coloneqq \mathsf{pf}_l^1(y) \times \mathsf{ef}_l(y) \tag{10}$$

$$\mathsf{pf}_l^1(y) \coloneqq \mathsf{pf}_l^0(y) \times \left(1 + \frac{\tau}{\mathcal{H}(x_l^\star, y) - \mathcal{H}(\bar{x}, y)}\right). \tag{11}$$

$$\mathsf{pf}_l^0(y) \coloneqq \|\nabla_x \mathcal{H}(x_l^\star, y)\|_S^2 \sqrt{\frac{\det \nabla_{xx}^2 \mathcal{H}(\bar{x}, y)}{2\pi\tau C_l^\star(y)}} \tag{12}$$

$$\mathsf{ef}_l(y) \coloneqq \exp\left[-\frac{\mathcal{H}(x_l^\star, y) - \mathcal{H}(\bar{x}, y)}{\tau}\right], \tag{13}$$

where $C_l^\star(y)$ is a factor accounting for the curvature of the failure surface in the vicinity of $x_l^\star$, and is given by:

$$C_l^\star(y) \coloneqq \nabla_x^\top \mathcal{H}(x_l^\star, y) \operatorname{adj}\left(X_l(y)\right) \nabla_x \mathcal{H}(x_l^\star, y) \tag{14}$$

$$X_l(y) \coloneqq \nabla_{xx}^2 \mathcal{H}(x_l^\star, y) - \mu_l^\star \nabla_{xx}^2 \Theta_l(x_l^\star, y), \tag{15}$$

where $\mu_l^\star \in \mathbb{R}$ is the optimal Lagrange multiplier in the constrained optimization problem (9).

In summary, the distribution of failure times for line $l \in \mathcal{L}'$ can be well-approximated by $T_l^\tau(y) \sim \mathrm{Exp}(\lambda_l^\tau(y))$, and therefore, the probability of observing line l fail in the first t seconds can be given by

$$\mathbb{P}(T_l^\tau(y) \leq t) = 1 - \exp\left[-\lambda_l^\tau(y) t\right]. \tag{16}$$

III. Failure Probability-constrained AC Optimal Power Flow Formulation

A. Conceptual formulation

The probability of transmission line failure (16) is a function of $y = \left(\{V_i\}_{i \in \mathcal{N} \setminus \mathcal{N}'}, \theta_\sigma, p_g, q_g\right)$, the voltage magnitudes at generator buses, the voltage angle at the slack bus and the active and reactive power generations. The choice of y also determines the equilibrium operating point $\bar{x}(y)$ through the power flow equations (4), (5); we shall denote these simply

[1]This assumption is not particularly restrictive since many high-voltage power transmission networks typically have resistance/reactance ratios below 0.2. Moreover, the standard DCOPF model for dispatch widely used in industry explicitly relies on this assumption [20]; in contrast, our model is far more general since we also consider nonlinearities, reactive powers and voltage magnitudes that the DCOPF model does not.

[2]Specifically, a singularly perturbed system of ordinary differential equations based on the swing equations and a frequency-dependent load model.

[3]We ignore the quadratic contribution $\frac{1}{2}\omega^\top M \omega$ from the frequency variables $\omega_i \coloneqq \dot{\theta}_i$ with mass M since the following sections ensure $\omega_i \equiv 0 \, \forall i$.

[4]This is not a strong assumption based on the validation in [18].

as $x = \big(\{V_i\}_{i\in\mathcal{N}'}, \{\theta_i\}_{i\in\mathcal{N}\setminus\{\sigma\}}\big)$ and along with the vector y, they constitute decision variables in our Failure Probability-constrained ACOPF (FP-ACOPF) formulation:

$$\underset{x,y}{\text{minimize}} \ \sum_{k\in\mathcal{G}} c_k(p_{g,k}) \tag{17}$$

subject to (4) − (5),

$$p_{g,k}^{\min} \le p_{g,k} \le p_{g,k}^{\max}, \ \ k \in \mathcal{G}, \tag{18}$$

$$q_{g,k}^{\min} \le q_{g,k} \le q_{g,k}^{\max}, \ \ k \in \mathcal{G}, \tag{19}$$

$$V_i^{\min} \le V_i \le V_i^{\max}, \ \ i \in \mathcal{N}, \tag{20}$$

$$\Theta_l(x,y) \le (I_l^{\lim})^2, \ \ l \in \mathcal{L}, \tag{21}$$

$$\lambda_l^{\tau}(y) \le \lambda_l^{\lim} := -t_H^{-1} \log\left(1-\epsilon_l^{\lim}\right), l \in \mathcal{L}' \tag{22}$$

The objective function (17) minimizes the cost of generation where c_k is a function representing the cost of generating active power $p_{g,k}$ at generator $k \in \mathcal{G}$. The constraints (18), (19) and (20) ensure that the power generations and voltage magnitudes stay within predefined limits. The constraint (21) limits the amount of current flow on the transmission lines, where we have distinguished the flow limit $I_l^{\lim}$ from the value I_l^{trip} used in the failure model (1). The latter quantity is the value at which protection relays would automatically disconnect the line, and it is typically much larger than the former, which is determined based on thermal considerations. Finally, constraint (22) imposes an upper bound on the failure rate of line $l \in \mathcal{L}'$, which by definition, is equivalent to delaying its expected failure time to be greater than $\left(\lambda_l^{\lim}\right)^{-1}$.

Observe that, using expression (16), the failure rate constraint (22) is equivalent to a chance constraint which ensures that the probability of line $l \in \mathcal{L}'$ failing over a time horizon t_H is less than some operator-prescribed limit $\epsilon_l^{\lim}$ (say 1%):

$$\mathbb{P}(T_l^{\tau}(y) \le t_H) \le \epsilon_l^{\lim}, \ \ l \in \mathcal{L}'. \tag{23}$$

We highlight that constraint (23) can be used as a safe approximation for limiting the probability of *(i)* non-independent failures (using Bonferroni's inequality), as well as *(ii)* cascading failures involving more than one line, over the horizon t_H. Indeed, while it is possible to constrain the *exact* probability of any cascading failure *sequence* of lines to stay below a certain risk threshold (since failure times are exponential random variables), the left-hand side of (23) can also be viewed as an upper bound on the probability of all such failure sequences that are initiated with the tripping of line l.

The presented model is a standard ACOPF formulation with the exception of the *failure rate constraint* (22). We now present an efficient reformulation of these rate constraints that can be incorporated into standard optimization solvers.

B. Reformulation of failure rate constraints: Key steps

Constraining the failure rate via (22) is nontrivial because it involves *(i)* the solution of a nested nonconvex optimization problem (9) to obtain $x_l^\star(y)$, and *(ii)* constraints involving determinants of large matrices, namely $\nabla_{xx}^2\mathcal{H}(x,y)$ and $X_l(y)$, see (12) and (14). This section shows that these can be circumvented by exploiting the low-rank property of the line failure function Θ_l, and a partial Talyor expansion of the energy function $\mathcal{H}$ around the equilibrium operating point x.

1) Low rank factorization of failure function: We shall capitalize on the fact that, the Hessian of the failure function Θ_l admits a low-rank factorization of the form:

$$\nabla_{xx}^2\Theta_l(x,y) = Q_l(x,y)\, K_l(x,y)\, Q_l^{\top}(x,y), \tag{24}$$

where $Q_l(x,y)$ is a $d\times r_l$ matrix, with $r_l \ll m$ and $K_l(x,y)$ is a $r_l \times r_l$ diagonal matrix. Observe that this low-rank structure is natural whenever Θ_l is a function of a small number of state variables, as is the case when Θ_l models the failure of transmission lines, system buses, generators or transformers.

Although such a low-rank factorization can be computed numerically (*e.g.*, using an eigenvalue decomposition), it can also be obtained analytically in several cases, such as in the examples of Section II-B. To illustrate this, Appendix A presents explicit closed-form expressions for Q_l and K_l when Θ_l is the line overcurrent function (1). In particular, it shows that $r_l = 3$ for a line $l = (i,j)$ where both $i,j \in \mathcal{N}'$ are non-generator buses, whereas $r_l = 2$ otherwise. The fact that the rank $r_l \le 3$ has nothing to do with the specific functional form of (1); in fact, $r_l \le 3$ will always hold whenever Θ_l is a function only of V_i, V_j and the angle difference $\theta_i - \theta_j$.

2) Taylor approximation of energy function: The value of the energy function at the most likely failure point, $\mathcal{H}(x_l^\star, y)$, is approximated using a quadratic Taylor polynomial centered around the equilibrium operating point x that is determined by the ACOPF formulation:

$$\mathcal{H}(x_l^\star,y) = \mathcal{H}(x,y) + \frac{1}{2}(x_l^\star - x)^{\top}\nabla_{xx}^2\mathcal{H}(x,y)(x_l^\star - x) \tag{25}$$

where we have ignored the first-order term since the FP-ACOPF constrains x to satisfy the power flow equations (4), (5), which are equivalent to $\nabla_x\mathcal{H}(x,y) = 0$. We shall comment on the accuracy of (25) in the next subsection.

C. Reformulation of the 'most likely failure point' problem

Equations (24) and (25) can be used to reformulate the nested nonconvex *most likely failure point* optimization problem (9). In particular, the following proposition shows that they can be used to generate tractable algebraic constraints under which the solution of (9) can be characterized by its first- and second-order optimality conditions

Proposition 1. *Fix a line $l \in \mathcal{L}'$, and assume that $x, x_l^\star \in \mathbb{R}^d$ and $y \in \mathbb{R}^{m-d}$ are such that:*

1) $\nabla_{xx}^2\mathcal{H}(x,y) \succ 0$, and

2) the Taylor approximation (25) *is applicable.*

If $x_l^\star$ and $\mu_l^\star \ge 0$ satisfy (26)–(28)*, then $x_l^\star$ is a local solution of the optimization problem* (9)*.*

$$\nabla_{xx}^2\mathcal{H}(x,y)(x_l^\star - x) = \mu_l^\star\nabla_x\Theta_l(x_l^\star,y) \tag{26}$$

$$\Theta_l(x_l^\star,y) = \Theta_l^{\max} \tag{27}$$

$$\mu_l^\star\,\rho\,(A_l) < 1, \tag{28}$$

where $A_l := K_l(x_l^\star,y)\,Q_l^{\top}(x_l^\star,y)\,[\nabla_{xx}^2\mathcal{H}(x,y)]^{-1}\,Q_l(x_l^\star,y)$ is a $r_l \times r_l$ matrix.

Proof. See Appendix B. □

Equations (26) and (27) are the first-order optimality conditions, whereas the spectral inequality (28) is derived from the

second-order optimality condition of the nested problem (9). It is noteworthy that the matrix A_l in the left-hand side of the latter inequality is a small $r_l \times r_l$ matrix, and hence it is possible to reformulate the inequality in a completely algebraic form without requiring a numerical eigenvalue computation.

When $r_l = 2$, it can be verified (*e.g.*, using the characteristic polynomial of A_l) that inequality (28) is equivalent to:

$$\mu_l^\star \operatorname{tr}(A_l) - (\mu_l^\star)^2 \det(A_l) < 1, \tag{29}$$

where the trace and determinant can be computed in algebraic closed-form, since A_l is a 2×2 matrix.

When $r_l = 3$, it is nontrivial to get a tractable reformulation, since A_l need not be symmetric. We consider two cases.

- If $K_l(x_l^\star, y) \succ 0$, then $\mu_l^\star \rho(A_l) < 1$ is equivalent to $\mu_l^\star \rho(\hat{A}_l) < 1$, $\hat{A}_l \coloneqq K_l^{\frac{1}{2}} Q_l^\top [\nabla_{xx}^2 \mathcal{H}(x,y)]^{-1} Q_l K_l^{\frac{1}{2}}$. This is a symmetric matrix, and hence, we can use Sylvester's criterion to enforce that all r_l leading principal minors of $I - \mu_l^\star \hat{A}_l$ (which are computable in algebraic closed-form) must be positive. A similar trick can be used if $K_l(x_l^\star, y)$ is negative definite.
- If $K_l(x_l^\star, y)$ is indefinite, then it is difficult to enforce the spectral inequality, and we settle for a relaxation which enforces a constraint on the sum of its r_l eigenvalues:

$$\mu_l^\star \operatorname{tr}(A_l) < r_l, \tag{30}$$

  where again the trace can be computed in closed-form.

We close with some remarks on the assumptions of Proposition 1. The first assumption requires that the Hessian of the energy function at the equilibrium point x is positive definite. Note that it is satisfied whenever x is obtained via the energy minimization problem (6). Although using the power flow equations (4), (5) as a surrogate for the latter cannot guarantee this condition, we found that it was almost never violated in our experiments. With regards to the second assumption, the Taylor approximation (25) is guaranteed to be accurate only when $x_l^\star$ is near x. We provide empirical evidence in Section IV that the approximation is not severe.

D. Treatment of high-dimensional determinants

Using equations (10) and (11), the failure rate constraint (22) can be equivalently written as:

$$\lambda_l^\tau(y) = \mathsf{pf}_l^0(y) \cdot \mathsf{ef}_l(y) \cdot \left(1 + \frac{\tau}{\mathcal{H}(x_l^\star, y) - \mathcal{H}(\bar{x}, y)}\right) \leq \lambda_l^{\lim}.$$

The formula for the prefactor $\mathsf{pf}_l^0(y)$ that appears in the above constraint involves determinants of (the typically large) $d \times d$ matrices, $\nabla_{xx}^2 \mathcal{H}(x,y)$ and $X_l(y)$, via (12) and (14) respectively. The presence of these determinants can slow down computation of the rate constraints and their gradients, and may result in ill-conditioning. Fortunately, equations (24) and (25) can be used to circumvent these issues. The following proposition uses the matrix-determinant lemma [29] to obtain a reformulation of the prefactor that avoids large determinants.

Proposition 2. *Fix a line $l \in \mathcal{L}'$, and assume that $x, x_l^\star \in \mathbb{R}^d$ and $y \in \mathbb{R}^{m-d}$ satisfy the conditions of Proposition 1. If $x_l^\star$ and $\mu_l^\star \geq 0$ satisfy* (26)–(28)*, then the prefactor and energy factor in equation* (10) *admit the following reformulation:*

$$\mathsf{pf}_l^1(y) = \mathsf{pf}_l^0(y) \left(1 + \frac{2\tau}{\mu_l^\star \alpha_l}\right) \tag{31}$$

$$\mathsf{pf}_l^0(y) = \frac{(\mu_l^\star)^{3/2} \|\nabla_x \Theta_l(x_l^\star, y)\|_S^2}{\sqrt{2\pi\tau\,(\alpha_l \det(W_l) + \beta_l)}} \tag{32}$$

$$\mathsf{ef}_l(y) = \exp\left(-\frac{\mu_l^\star \alpha_l}{2\tau}\right), \tag{33}$$

where $W_l \coloneqq I - \mu_l^\star A_l$ is a $r_l \times r_l$ matrix, A_l is as in Proposition 1, and the scalars $\alpha_l \coloneqq (x_l^\star - x)^\top \nabla_x \Theta_l(x_l^\star, y)$ and $\beta_l \coloneqq (x_l^\star - x)^\top Q_l(x_l^\star, y) \operatorname{adj}(W_l) K_l(x_l^\star, y) Q_l^\top(x_l^\star, y)(x_l^\star - x)$.

Proof. See Appendix C. □

Unlike equations (12) and (14), equation (32) involves the determinant and adjugate of the small $r_l \times r_l$ matrix W_l. This allows efficient computation of the scalar β_l, and hence, of the overall failure rate and its gradient. Moreover, it avoids the ill-conditioning that plagues the original constraint, and allows expressing it in an algebraic optimization system.

E. Efficient practical implementation

We now highlight other key algorithmic enhancements that are necessary to improve the practical performance of the FP-ACOPF. First, since the absolute value of the failure rates $\lambda_l^\tau(y)$ can be very small, we found it beneficial to implement the rate constraint (22) in its log-form. Using equations (10), and (31)–(33), this is equivalent to:

$$\frac{3}{2}\log(\mu_l^\star) + \log\left(\|\nabla_x \Theta_l(x_l^\star, y)\|_S^2\right) - \frac{1}{2}\log\left(\alpha_l \det(W_l) + \beta_l\right) + \log\left(1 + \frac{2\tau}{\mu_l^\star \alpha_l}\right) - \frac{\mu_l^\star \alpha_l}{2\tau} \leq \log(\sqrt{2\pi\tau}\lambda_l^{\lim}). \tag{34}$$

All intermediate terms involved in the left-hand side of (34) are computable in closed form, except for the matrix A_l which appears in the definition of $W_l \coloneqq I - \mu_l^\star A_l$. A close examination of the formula for A_l in Proposition 1 reveals that this matrix can be efficiently constructed by first solving for the intermediate matrix $Z_l \in \mathbb{R}^{d \times r_l}$ as follows:

$$\nabla_{xx}^2 \mathcal{H}(x,y) \cdot Z_l = Q_l(x_l^\star, y), \tag{35}$$

and then setting $A_l = K_l(x_l^\star, y) Q_l^\top(x_l^\star, y) Z_l$. We therefore introduce explicit decision variables Z_l, along with (35) as constraints in the FP-ACOPF formulation. Notably, this allows the complete rate constraint (34), including all of its intermediate expressions, to be computed algebraically.

Implementing the rate constraint (22) for a particular line $l \in \mathcal{L}'$ thus involves introducing $dr_l + d + 1$ additional variables, namely $Z_l \in \mathbb{R}^{d \times r_l}$, $x_l^\star \in \mathbb{R}^d$ and $\mu_l^\star \geq 0$ and $dr_l + d + 3$ additional constraints, namely (26)–(28) and (34)–(35). In practice, the rate constraints (34) are binding for only a small fraction of critical lines. Therefore, adding $\mathcal{O}(dr_l)$ constraints for the remaining non-critical lines unnecessarily increases model complexity. To limit this growth, we add additional variables and constraints in an iterative manner, only for those lines $l \in \hat{\mathcal{L}}$ whose rate constraints (34) are found to be violated. Our algorithm can be described as follows.

Step 1: Set $\hat{\mathcal{L}} = \emptyset$.

Step 2: Define decision variables $x \in \mathbb{R}^d$, $y \in \mathbb{R}^{m-d}$, and $\left\{(x_l^\star, \mu_l^\star, Z_l) \in \mathbb{R}^d \times \mathbb{R}_{\geq 0} \times \mathbb{R}^{d \times r_l}\right\}$ for each $l \in \hat{\mathcal{L}}$. Compute an optimal solution $\hat{z}$ of the problem:

$$\begin{aligned} &\text{minimize} && (17) \\ &\text{subject to} && (4), (5), (18) - (21), \\ & && (26) - (28), (34), (35) \ \ \forall l \in \hat{\mathcal{L}}. \end{aligned}$$

Step 3: For all $l \in \mathcal{L}' \setminus \hat{\mathcal{L}}$ (possibly in parallel):

a) Use $\hat{z}$ to compute candidate values of $x_l^\star, \mu_l^\star, Z_l$ by solving equations (26)-(28), and (35).

b) If inequality (34) is violated using $\hat{z}$ and the computed values of $x_l^\star, \mu_l^\star, Z_l$, update $\hat{\mathcal{L}} = \hat{\mathcal{L}} \cup \{l\}$ and save the computed values as warm-starts.

Step 4: If $\hat{\mathcal{L}}$ was updated, go to Step 2; else, stop and output $(\hat{x}, \hat{y})$ as the optimal FP-ACOPF solution.

IV. Numerical Simulations

We now present results and insights obtained from several experiments.[5] The IEEE 118-bus test system with line limits $I_l^{\lim}$ obtained from PGLib [30], is used in all experiments. We set branch and shunt conductances to zero to satisfy the lossless assumption[6], remove transmission line taps for simplicity, and set the system matrices J and S that appear in (2) as per [31]. The numerical performance of the FP-ACOPF is largely unaffected by the choice of the noise parameter τ, the line failure threshold I_l^{trip}, and the network loading (p_d, q_d) levels. Therefore, Section IV-A uses 'baseline' values of $\tau = 10^{-4}$, $I_l^{\text{trip}} = 1.02\, I_l^{\max}$ and (p_d, q_d) values from MATPOWER [32]. Their values can, however, strongly affect cascading behavior; therefore, Section IV-B includes a discussion of cascading sensitivity to their values.

A. Computational efficiency of FP-ACOPF

For a fixed dispatch point y, the true line failure rates $\lambda_l^\tau(y)$ are computed by solving problem (9) to obtain the most likely failure point $x_l^\star$ and its multiplier $\mu_l^\star$. However, the FP-ACOPF computes an estimate, which we denote as $\tilde{\lambda}_l^\tau(y)$, by solving (26)–(28) instead of (9). Fig. 1a shows the corresponding approximation error for the subset of lines with the highest failure rates. We observe that the relative log-error in the approximation is less than 10^{-2}. Fig. 1b shows that lines with higher utilization of their flow capacity, defined as $\sqrt{\Theta_l(x,y)}/I_l^{\lim} \times 100\%$, do not necessarily have higher failure rates, thus illustrating that *the magnitude of line flow is not an effective surrogate for its failure rate*. For example the line with the second-largest capacity utilization has a failure rate in the middle of the range, whereas lines with the largest failure rates have capacity utilization close to 50%. For accuracy, we must thus work directly with the failure rates via (10).

[5]Our Julia code is available at: github.com/jacob-roth/OPF. All optimization problems were solved using Ipopt via JuMP. The runs were performed on 32 threads of an Intel Xeon Gold 6140 CPU at 2.30GHz with 512 GB RAM.

[6]For some context on this assumption, the mean branch resistance/reactance ratio is approximately 0.2. Also, the mean difference between the ACOPF solutions computed with and without resistances is 0.004 p.u. and 0.04 for the voltage magnitudes and angles, respectively.

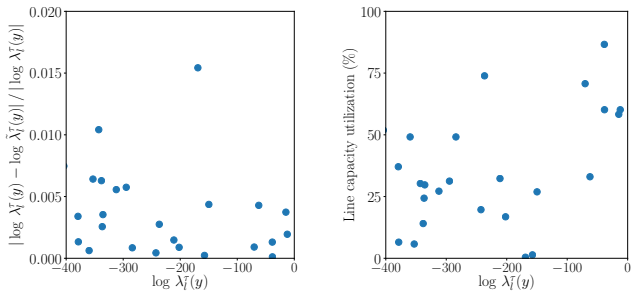

(a) Failure rate approximation error (b) Capacity utilization vs. failure rate

Fig. 1. Fig. 1a shows the relative log-error in approximating the true failure rate $\lambda_l^\tau(y)$ by $\tilde{\lambda}_l^\tau(y)$ in the rate-constrained model. Fig. 1b shows line capacity utilization as a function of its failure rate. Each dot corresponds to a transmission line and y is the classical (*i.e.*, $N-0$) ACOPF dispatch.

TABLE I
Summary of Numerical Performance

Formulation	$\max_{l \in \mathcal{L}'} \lambda_l^\tau(y)$	Solve time (sec)	Cost diff (%)
$N-0$	4.9×10^{-5}	0.2	–
$N-1$	2.5×10^{-5}	141.9	0.04
$\lambda^{\lim} = 10^{-9}$	9.8×10^{-10}	4.5	0.01
$\lambda^{\lim} = 10^{-12}$	9.8×10^{-13}	3.0	0.02
$\lambda^{\lim} = 10^{-15}$	9.9×10^{-16}	4.2	0.04

Table I summarizes the computational time and generation cost of the failure probability-constrained and $N-k$ security-constrained[7] dispatch points. We observe that the FP-ACOPF solves within an order of magnitude of the time it takes to solve the $N-0$ ACOPF. On the other hand, the $N-1$ model is slower by almost three orders of magnitude, although this may be because all contingencies are included in a single optimization problem. In terms of generation cost, including the rate constraints results in a cost increase of less than 1% compared to the $N-0$ model, even with extremely stringent rate limits, without requiring any load shedding.

B. Cascading failure simulations of FP-ACOPF dispatch

To compare the cascade potentials of the failure probability-constrained and $N-k$ security-constrained ACOPF, we perform $1,000$ Kinetic Monte Carlo (KMC) simulations [18] per dispatch point. The latter simulates cascading sequences of line failures for a given dispatch point, using the failure rate expression in (10). Similar to other quasi-steady-state models, it assumes that the system 're-equilibriates' immediately following an individual line failure; *i.e.*, the post-failure system state satisfies the power flow equations and hence, is a local minimizer (6) of the energy function, appropriately modified (via the admittance matrix) to account for the degraded network topology. Following each line failure, the slack bus is assumed to maintain power balance in the network, and buses that no longer connect to the slack bus (under the modified network topology) are 'deactivated'. The

[7]The set of contingencies is comprised of all lines, and post-contingency generation is allowed to vary by at most $0.1 p_{g,k}^{\max}$ at each generator $k \in \mathcal{G}$.

cumulative active demand p_d at deactivated buses serves as a measure of lost load. This enables fair comparison of different dispatch points, on the basis of time and severity until full system collapse or until a very large simulation time (10^{30} sec in our implementation) has elapsed.

Fig. 2 summarizes the simulation performance of the FP-ACOPF and $N-1$ security-constrained ACOPF, relative to the $N-0$ dispatch, for baseline values of $\tau = 10^{-4}$, $I_l^{\text{trip}} = 1.02\, I_l^{\max}$ and nominal MATPOWER (p_d, q_d). First, in Fig. 2a, we group the $1,000$ simulated line failure sequences into individual cascades as per [33] and then report the distribution of cascades as a function of the number of failed lines. We observe not only an approximate power law distribution (which serves as validation), but also–and more importantly–that the FP-ACOPF reduces the frequency of longer, more severe cascades. Unlike the $N-1$ model, it can be tuned via the rate limits $\lambda^{\lim}$, and for sufficiently stringent $\lambda^{\lim} = 10^{-15}$, it can prevent the occurrence of long cascades entirely.

To study this phenomenon more closely, in Figs. 2b and 2c, we plot the observed distribution (over the $1,000$ failure sequences) of elapsed time and total demand lost, as a function of number of line failures, respectively. These figures display a distribution of line failure sequences from separate KMC runs, in contrast to Fig. 2a which separates failure sequences into subsequences (cascades) based on the time between successive failures and plots the aggregate count of subsequences of a certain length. In these figures, one method dominates another if its failure time distribution in Fig. 2b lies above, and if its load lost distribution in Fig. 2c lies below that of the other. Fig. 2b shows that, by delaying the system's first failure time, the FP-ACOPF dispatch points are able to successfully delay–and hence, prevent–subsequent line failures which could lead to system collapse. Interestingly, all dispatch points display a long plateau of rapid consecutive failures following the first few failures, indicating dangerous system instability. The FP-ACOPF models seem to delay the onset of such instability and are thus able to find more 'stable' dispatch points; for example, the onset of the plateau in $\lambda^{\lim} = 10^{-15}$ is delayed by almost ten orders of magnitude, compared to $N-1$. Moreover, Fig. 2c shows that the fraction of load lost decreases almost monotonically with $\lambda^{\lim}$, indicating that reduced cascading risk is not accompanied with increased load shedding.

To study the sensitivity of our results to the choice of the noise parameter τ, line failure threshold I_l^{trip} and loads (p_d, q_d), we repeated our analysis by varying them as follows: $\tau \in \{\frac{1}{2}, 1, 2\} \times 10^{-4}$, $I_l^{\text{trip}} \in \{1.02, 1.05\} \times I_l^{\max}$ and $(p_d, q_d) \in \{0.9, 1, 1.1\}\times$ nominal MATPOWER values[8,9]. We found that the overall results were largely unaffected by the choice of I_l^{trip}, but were sensitive to the noise parameter τ and load levels (p_d, q_d), with cascade severity increasing monotonically with τ as well as (p_d, q_d). Moreover, we observed that the FP-ACOPF generally outperformed the $N-1$ ACOPF dispatch, both in terms of cascade severity and timing, across the range of parameter values we studied, and therefore, do not present detailed results for the sake of brevity. Importantly, this observation alleviates some of the practical concerns over specifying the values of these parameters precisely.

[8]Using the magnitude of frequency fluctuations in historical data, [34] estimates $\tau \approx 2.5m \times 10^{-4}$ for combined mass and damping parameter m. Since the dynamics model in [18] has $m \approx 0.05$, this suggests $\tau \approx 1.25 \times 10^{-5}$. To induce line failures, and since the noise model (2) has not yet been calibrated against real data, we simply experiment with various values of τ, and observe that $\tau \approx 10^{-4}$ gives reasonable failure behavior.

[9]In [6], emergency limits I_l^{trip} are set with a 25% buffer above their rating so that $I_l^{\text{trip}} = 1.25 \times I_l^{\max}$. Since the $N-0$ ACOPF dispatch point of the PGLib 118-bus case has a mean "factor of safety" of 3.9; *i.e.*, nominal line flows are 39% away from their (very loose) rated values, we reduce the traditional 25% buffer and consider more challenging conditions.

V. Conclusion and Future Work

This paper takes the first steps towards quantifying and proactively reducing failure risk, and, implicitly, cascading risk in operational dispatch. Our empirical results demonstrate that the failure rate limit $\lambda^{\lim}$ serves as an accurate, monotone and tunable metric of cascade severity, and the FP-ACOPF can strongly outperform classical $N-k$ models in terms of both the onset as well as severity of line failures, without incurring significantly larger computational or economic costs.

We envision future work along several directions. From a methodological viewpoint, we need to extend the failure probability model and the corresponding optimization model to lossy networks. From a modeling viewpoint, more general multiple-component failure rate constraints, as well as extensions that combine classical $N-1$ models with rate constraints at the inner level need to be investigated. From a practical viewpoint, the model parameters (e.g., τ) need to be calibrated and the model itself needs to be further validated and compared against established cascading simulators on real network data, with some initial steps already being taken in [18]. We believe these extensions can open up several other use cases for our method including long-term planning decisions, line capacity allocations, and contingency screening.

Appendix

A. Closed-form expressions of low-rank factors

Consider the line overcurrent function (1) for a line $l = (i, j)$. First, consider the case where both $i, j \in \mathcal{N}'$ are non-generator buses, so that $V_i, V_j, \theta_i, \theta_j$ are all part of the state vector x. In this case, $r_l = 3$ and only the rows of Q_l corresponding to these components have nonzero elements. Suppose $1_w \in \mathbb{R}^d$ is the canonical unit vector with 1 in the w-component and 0 otherwise. Then, it can be verified that $\nabla^2_{xx}\Theta_l = Q_l K_l Q_l^\top$, where $K_l = \operatorname{diag}(1, 1, -1)$ and the matrix Q_l is as follows:

1) $Q_l^\top 1_w = 0 \in \mathbb{R}^3$ for all $w \notin \{V_i, V_j, \theta_i, \theta_j\}$,
2) $Q_l^\top \begin{bmatrix} 1_{V_i} & 1_{V_j} & 1_{\theta_i} & 1_{\theta_j} \end{bmatrix}$ is given by:

$$\begin{bmatrix} 1 & -c_{ij} & V_j s_{ij} & -V_j s_{ij} \\ 0 & s_{ij} & V_i + V_j c_{ij} & -V_i - V_j c_{ij} \\ 0 & 0 & \sqrt{V_i^2 + V_j^2 + V_i V_j c_{ij}} & -\sqrt{V_i^2 + V_j^2 + V_i V_j c_{ij}} \end{bmatrix}$$

$$c_{ij} \coloneqq \cos(\theta_i - \theta_j), \quad s_{ij} \coloneqq \sin(\theta_i - \theta_j).$$

If $j \in \mathcal{N} \setminus (\mathcal{N}' \cup \{\sigma\})$ is a non-slack generator bus, then V_i, θ_i, θ_j are part of x, but not V_j. In this case, $r_l = 2$, $K_l = \operatorname{diag}\left(1, V_i V_j c_{ij} - V_j^2 s_{ij}^2\right)$ and, along with condition 1) described above, the matrix Q_l is characterized by:

$$Q_l^\top \begin{bmatrix} 1_{V_i} & 1_{\theta_i} & 1_{\theta_j} \end{bmatrix} = \begin{bmatrix} 1 & V_j s_{ij} & -V_j s_{ij} \\ 0 & 1 & -1 \end{bmatrix}$$

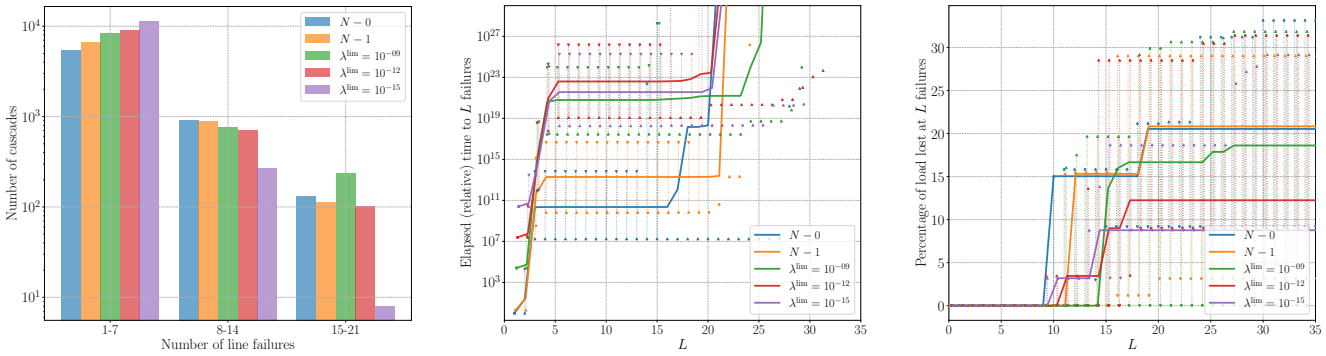

(a) Cascade size distribution (b) Failure time distribution (c) Load shed distribution

Fig. 2. Empirical distribution of (a) number of cascades, (b) elapsed time (in failure sequence), and (c) cumulative load lost (in failure sequence) as a function of number of line failures, for $\tau = 10^{-4}$, $I_l^{\text{trip}} = 1.02\, I_l^{\max}$ and nominal (p_d, q_d). In figures (b) and (c), the y-axis entries are normalized with respect to the corresponding entries for the $N-0$ ACOPF at 1 failure, and the line failure sequences are augmented so that failures that occur after 10^{30} are treated as ∞. The markers in Figs. 2b and 2c indicate "$\triangle$"–minimum, "solid line"–median, and "$\triangledown$"–maximum of the corresponding empirical distributions.

If $j = \sigma$ is the slack bus, then $r_l = 2$, and the above expressions for K_l and Q_l continue to be applicable, except θ_j is not part of x and has no corresponding column in Q_l.

B. Proof of Proposition 1

We drop the subscript l from all quantities to simplify the notation. First, observe that if $x^\star$ satisfies equation (27), *i.e.*, $\Theta(x^\star, y) = \Theta^{\max}$, then it must also satisfy $\nabla_x \Theta(x^\star, y) \neq 0$. Indeed, by definition of Θ in (1), it follows that $\nabla_x \Theta(x^\star, y) = 0$ implies $V_i^\star = V_j^\star = 0$. This, in turn, implies $\Theta(x^\star, y) = 0$, which is a contradiction $\Theta^{\max} > 0$. Hence, $\nabla_x \Theta(x^\star, y) \neq 0$, and the *linearly independent constraint qualification* is satisfied for problem (9) at $x^\star$. Therefore, its first-order optimality conditions, which are (26) using the Taylor approximation (25) and equation (27), must be necessarily satisfied at $x^\star$.

Now, consider the Hessian of the Lagrangian of problem (9) at the primal-dual pair $(x^\star, \mu^\star)$: $M := \nabla^2_{xx}\mathcal{H}(x, y) - \mu^\star \nabla^2_{xx}\theta(x^\star, y)$, where again we have used the Taylor approximation (25). Along with the first-order conditions, the second-order sufficient conditions ensure that, if $M \succ 0$, then $x^\star$ is a local solution of problem (9). In the following paragraph, we show that $M \succ 0$ is equivalent to condition (28).

Denote $\nabla^2\mathcal{H} := \nabla^2_{xx}\mathcal{H}(x, y)$, $Q^\star := Q(x^\star, y)$ and $K^\star := K(x^\star, y)$. Using factorization (24) and by using the hypothesis $\nabla^2\mathcal{H} \succ 0$ in the statement of the Proposition, we have

$$\begin{aligned}
&M = \nabla^2\mathcal{H} - \mu^\star Q^\star K^\star (Q^\star)^\top \succ 0 \\
\iff &I - \mu^\star [\nabla^2\mathcal{H}]^{-1/2} Q^\star K^\star (Q^\star)^\top [\nabla^2\mathcal{H}]^{-1/2} \succ 0 \\
\iff &\mu^\star \rho\left([\nabla^2\mathcal{H}]^{-1/2} Q^\star K^\star (Q^\star)^\top [\nabla^2\mathcal{H}]^{-1/2}\right) < 1 \\
\iff &\mu^\star \rho\left(K^\star (Q^\star)^\top [\nabla^2\mathcal{H}]^{-1} Q^\star\right) < 1.
\end{aligned}$$

where the last equivalence from the fact that the non-zero eigenvalues of AB coincide with those of BA for arbitrary matrices A and B of appropriate size.

C. Proof of Proposition 2

We again drop the subscript l from all quantities to simplify notation. Using equations (25) and (26), we obtain:

$$\begin{aligned}
\mathcal{H}(x^\star, y) - \mathcal{H}(x, y) &= \frac{1}{2}(x^\star - x)^\top \nabla^2_{xx}\mathcal{H}(x, y)(x^\star - x) \\
&= \frac{1}{2}\mu^\star (x^\star - x)^\top \nabla_x \Theta(x^\star, y) = \frac{1}{2}\mu^\star \alpha,
\end{aligned}$$

which shows the validity of (31) and (33).

Denote $\nabla^2\mathcal{H} := \nabla^2_{xx}\mathcal{H}(x, y)$, $Q^\star := Q(x^\star, y)$ and $K^\star := K(x^\star, y)$. To show validity of (32), we will show that equation (14) simplifies to $C^\star(y) = \mu^\star \det(\nabla^2\mathcal{H})\,(\alpha \det(W) + \beta)$. The factorization (24) and Taylor approximation (25) imply that (15) is equivalent to $X(y) = \nabla^2\mathcal{H} - \mu^\star Q^\star K^\star (Q^\star)^\top$. Furthermore, the proof of Proposition 1 shows that $X(y) \succ 0$ and hence, that it is invertible. Therefore, we have

$$\operatorname{adj}(X(y)) = [X(y)]^{-1} \det(X(y)).$$

Since $\nabla^2\mathcal{H} \succ 0$, we can use the Woodbury identity to obtain:

$$[X(y)]^{-1} = \left[\nabla^2\mathcal{H}\right]^{-1} + \left[\nabla^2\mathcal{H}\right]^{-1} \mu^\star Q^\star W K^\star (Q^\star)^\top \left[\nabla^2\mathcal{H}\right]^{-1}$$

Similarly, application of [29, Theorem 18.1.1] gives:

$$\det(X(y)) = \det(\nabla^2\mathcal{H}) \det(W)$$

Equation (25) implies $\nabla\mathcal{H}^\star(y) = \nabla^2\mathcal{H} \cdot (x^\star - x)$, and along with the above equations, this simplifies (14) as follows:

$$\begin{aligned}
C^\star(y) &= \nabla^\top \mathcal{H}^\star(y) \operatorname{adj}(X(y)) \nabla\mathcal{H}^\star(y) \\
&= \det(\nabla^2\mathcal{H}) \det(W) \cdot \Big\{(x^\star - x)^\top \nabla^2\mathcal{H}\,(x^\star - x) \\
&\qquad + \mu^\star (x^\star - x)^\top Q^\star W K^\star (Q^\star)^\top (x^\star - x)\Big\} \\
&= \mu^\star \det(\nabla^2\mathcal{H})\,(\alpha \det(W) + \beta)
\end{aligned}$$

where the last equality follows from equation (26) and the definition of α and β.

REFERENCES

[1] R. Baldick, B. Chowdhury, I. Dobson, Z. Dong, B. Gou, D. Hawkins, H. Huang, M. Joung, D. Kirschen, F. Li *et al.*, "Initial review of methods for cascading failure analysis in electric power transmission systems ieee pes cams task force on understanding, prediction, mitigation and restoration of cascading failures," in *2008 IEEE Power and Energy Society General Meeting*. IEEE, 2008, pp. 1–8.

[2] H. Guo, C. Zheng, H. H.-C. Iu, and T. Fernando, "A critical review of cascading failure analysis and modeling of power system," *Renewable and Sustainable Energy Reviews*, vol. 80, pp. 9–22, 2017.

[3] P. Hines and S. Blumsack, "A centrality measure for electrical networks," in *Proceedings of the 41st Annual Hawaii International Conference on System Sciences (HICSS 2008)*. IEEE, 2008, pp. 185–185.

[4] C. D. Brummitt, R. M. D'Souza, and E. A. Leicht, "Suppressing cascades of load in interdependent networks," *Proceedings of the National Academy of Sciences*, vol. 109, no. 12, pp. E680–E689, 2012.

[5] J. Yan, Y. Tang, H. He, and Y. Sun, "Cascading failure analysis with dc power flow model and transient stability analysis," *IEEE Transactions on Power Systems*, vol. 30, no. 1, pp. 285–297, 2014.

[6] P. Henneaux, E. Ciapessoni, D. Cirio, E. Cotilla-Sanchez, R. Diao, I. Dobson, A. Gaikwad, S. Miller, M. Papic, A. Pitto *et al.*, "Benchmarking quasi-steady state cascading outage analysis methodologies," in *2018 IEEE International Conference on Probabilistic Methods Applied to Power Systems (PMAPS)*. IEEE, 2018, pp. 1–6.

[7] C. L. DeMarco, "A phase transition model for cascading network failure," *IEEE Control Systems Magazine*, vol. 21, no. 6, pp. 40–51, 2001.

[8] J. Song, E. Cotilla-Sanchez, G. Ghanavati, and P. D. Hines, "Dynamic modeling of cascading failure in power systems," *IEEE Transactions on Power Systems*, vol. 31, no. 3, pp. 2085–2095, 2015.

[9] B. Schäfer, D. Witthaut, M. Timme, and V. Latora, "Dynamically induced cascading failures in power grids," *Nature communications*, vol. 9, no. 1, pp. 1–13, 2018.

[10] I. Dobson, B. A. Carreras, and D. E. Newman, "A loading-dependent model of probabilistic cascading failure," *Probability in the Engineering and Informational Sciences*, vol. 19, no. 1, p. 15, 2005.

[11] M. Rahnamay-Naeini, Z. Wang, N. Ghani, A. Mammoli, and M. M. Hayat, "Stochastic analysis of cascading-failure dynamics in power grids," *IEEE Transactions on Power Systems*, vol. 29, no. 4, pp. 1767–1779, 2014.

[12] D. Bienstock, "Optimal control of cascading power grid failures," in *2011 50th IEEE Conference on Decision and Control and European Control Conference*. IEEE, 2011, pp. 2166–2173.

[13] A. Esmaeilian and M. Kezunovic, "Prevention of power grid blackouts using intentional islanding scheme," *IEEE transactions on industry applications*, vol. 53, no. 1, pp. 622–629, 2016.

[14] L. Guo, C. Liang, A. Zocca, S. H. Low, and A. Wierman, "Localization & Mitigation of Cascading Failures in Power Systems, Part III: Real-time Mitigation," *arXiv preprint arXiv:2005.11319*, 2020.

[15] H. Wang and J. S. Thorp, "Optimal locations for protection system enhancement: a simulation of cascading outages," *IEEE Transactions on Power Delivery*, vol. 16, no. 4, pp. 528–533, 2001.

[16] R. C. Hardiman, M. Kumbale, and Y. V. Makarov, "An advanced tool for analyzing multiple cascading failures," in *2004 International Conference on Probabilistic Methods Applied to Power Systems*. IEEE, 2004, pp. 629–634.

[17] J. Qi, K. Sun, and S. Mei, "An interaction model for simulation and mitigation of cascading failures," *IEEE Transactions on Power Systems*, vol. 30, no. 2, pp. 804–819, 2014.

[18] J. Roth, D. A. Barajas-Solano, P. Stinis, J. Weare, and M. Anitescu, "A kinetic monte carlo approach for simulating cascading transmission line failure," *arXiv preprint arXiv:1912.08081*, 12 2019.

[19] H. Zheng and C. L. DeMarco, "A bi-stable branch model for energy-based cascading failure analysis in power systems," *North American Power Symposium 2010*, pp. 1–7, 2010.

[20] B. Stott, J. Jardim, and O. Alsaç, "Dc power flow revisited," *IEEE Transactions on Power Systems*, vol. 24, no. 3, pp. 1290–1300, 2009.

[21] C. DeMarco and A. Bergen, "A security measure for random load disturbances in nonlinear power system models," *IEEE Transactions on Circuits and Systems*, vol. 34, no. 12, pp. 1546–1557, 12 1987.

[22] A. R. Bergen and D. J. Hill, "A structure preserving model for power system stability analysis," *IEEE Transactions on Power Apparatus and Systems*, vol. PAS-100, no. 1, pp. 25–35, 1 1981.

[23] C. L. DeMarco and A. R. Bergen, "Application of singular perturbation techniques to power system transient stability analysis," in *Proceedings of the International Symposium on Circuits and Systems*, 1984, pp. 597–601.

[24] C. L. DeMarco and A. R. Bergen, "Small noise in power system dynamics and its relation to security assessment," in *1985 American Control Conference*, 6 1985, pp. 559–560.

[25] M. Pai, *Energy function analysis for power system stability*. Springer Science & Business Media, 2012.

[26] A. Fouad and V. Vittal, "The transient energy function method," *International Journal of Electrical Power & Energy Systems*, vol. 10, no. 4, pp. 233–246, 1988.

[27] M. I. Freidlin and A. D. Wentzell, *Random Perturbations of Dynamical Systems*, 3rd ed. Springer-Verlag Berlin Heidelberg, 2012, vol. 260.

[28] P. Collet, S. Martínez, and J. San Martín, *Quasi-Stationary Distributions: General Results*. Berlin, Heidelberg: Springer Berlin Heidelberg, 2013, pp. 17–29.

[29] D. A. Harville, *Matrix Algebra From a Statistician's Perspective*. Springer New York, 2008.

[30] S. Babaeinejadsarookolaee *et al.*, "The Power Grid Library for Benchmarking AC Optimal Power Flow Algorithms," *arXiv e-prints*, 8 2019.

[31] H. Zheng and C. L. DeMarco, "A new dynamic performance model of motor stalling and fidvr for smart grid monitoring/planning," *IEEE Transactions on Smart Grid*, vol. 7, no. 4, pp. 1989–1996, July 2016.

[32] R. D. Zimmerman, C.E. Murillo-Sanchez, and R. J. Thomas, "Matpower: Steady-state operations, planning and analysis tools for power systems research and education," pp. 12–19, 2 2011.

[33] I. Dobson, "Estimating the propagation and extent of cascading line outages from utility data with a branching process," *IEEE Transactions on Power Systems*, vol. 27, no. 4, pp. 2146–2155, 11 2012.

[34] C. Matthews, B. Stadie, J. Weare, M. Anitescu, and C. Demarco, "Simulating the stochastic dynamics and cascade failure of power networks," 6 2018.

Anirudh Subramanyam is a postdoctoral researcher in the Mathematics and Computer Science Division at Argonne National Laboratory. He obtained his bachelor's degree from the Indian Institute of Technology, Bombay and his Ph.D. from Carnegie Mellon University, both in chemical engineering. His research interests are in computational methods for nonlinear and discrete optimization under uncertainty with applications in energy, transportation and process systems.

Jacob Roth received his M.S. degree from the University of Chicago and worked at Argonne National Laboratory as a pre-doctoral appointee for two years. Currently he is a Ph.D. candidate at the University of Minnesota and is interested in computational mathematics.

Mihai Anitescu is a senior computational mathematician in the Mathematics and Computer Science Division at Argonne National Laboratory and a professor in the Department of Statistics at the University of Chicago. He obtained his engineer diploma (electrical engineering) from the Polytechnic University of Bucharest in 1992 and his Ph.D. in applied mathematical and computational sciences from the University of Iowa in 1997. He specializes in the areas of numerical optimization, computational science, numerical analysis and uncertainty quantification in which he has published more than 100 papers in scholarly journals and book chapters. He is on the editorial board of the SIAM Journal on Optimization and he is a senior editor for Optimization Methods and Software, he is a past member of the editorial boards of the Mathematical Programming A and B, SIAM Journal on Uncertainty Quantification, and SIAM Journal on Scientific Computing. He has been recognized for his work in applied mathematics by his selection as a SIAM Fellow in 2019.